ERJ Express. Published on March 21, 2013 as doi: 10.1183/09031936.00182412

Ex vivo µCT analysis of bleomycin-induced lung fibrosis for pre-clinical drug evaluation

Chris J. Scotton[1#], Brian Hayes[2], Robert Alexander[1], Arnab Datta[1], Ellen J Forty[1], Paul F. Mercer[1], Andy Blanchard[2] and Rachel C. Chambers[1]

[1]Centre for Inflammation and Tissue Repair, UCL Respiratory, University College London, London, UK

[2]Fibrosis DPU, GlaxoSmithKline, Stevenage, UK

#Author for correspondence at the above address:

Tel +44 (0)207 679 6276; Fax +44 (0)207 679 6973; Email: c.scotton@ucl.ac.uk

Running title: µCT analysis of experimental lung fibrosis

Word count: 3780

ABSTRACT

Research question

Research into the pathogenesis underlying the development of idiopathic pulmonary fibrosis (IPF) is hampered by a repertoire of animal models which fail to recapitulate all the features of the human disease. Better use and understanding of what the animal models represent may improve clinical predictability. We interrogated *ex vivo* micro-Computed Tomography (μCT) as a novel endpoint measure in the mouse model of bleomycin-induced lung fibrosis (BILF), and to evaluate a therapeutic dosing regimen for pre-clinical drug evaluation.

Methods

A detailed characterisation of BILF was performed using standard endpoint measures (lung hydroxyproline and histology). High resolution μCT (~13.7 μm voxel size) was evaluated for quantifying the extent and severity of lung fibrosis.

Results

The period from 14 to 28 days following bleomycin instillation represents progression of established fibrosis. A therapeutic dosing regimen during this period was validated using a TGFβR1 kinase inhibitor, and μCT provided a highly sensitive and quantitative measure of fibrosis. Moreover, fibrotic lesions did not completely resolve, but instead persisted for at least six months following a single insult with bleomycin.

Conclusions

Ex vivo µCT analysis of BILF allows robust evaluation of therapeutic dosing once fibrosis is already well-established, requiring fewer mice than conventional biochemical endpoints.

Key words:

Bleomycin, idiopathic pulmonary fibrosis, micro-CT, resolution, therapy

Summary (in 130 characters or less)

Micro-CT has improved our understanding of the bleomycin model of fibrotic lung disease for pre-clinical drug evaluation.

INTRODUCTION

Idiopathic Pulmonary Fibrosis (IPF) is a chronic, progressive and ultimately fatal condition, characterised by the excessive deposition of extracellular matrix and destruction of the lung architecture. In the USA and Europe there are currently in excess of 500,000 IPF patients [1], who place a significant clinical and financial burden on healthcare systems. Disease progression is generally refractory to current pharmacological interventions, resulting in a median survival of 3 – 5 years following diagnosis [2]. Identification of novel therapeutic interventions is therefore paramount to supplement the extremely limited repertoire of drugs which have shown signs of clinical benefit.

Experimental lung fibrosis models are routinely used for the identification of relevant underlying pathomechanisms and assessment of drug efficacy. IPF research is, however, hampered by animal models which do not recapitulate all the features of the human disease, and whose ability to predict future clinical outcomes has been questioned. From the plethora of pathways/targets which show anti-fibrotic potential in these experimental models, few have gone on to show benefit in clinical trials (see [3] for an excellent review). Several different models exist [4], of which lung fibrosis induced by bleomycin (bleo) application is probably the best characterised and most widely utilised, although there is no accepted standardised version of this model [5]. A variety of factors will affect the nature of the fibrotic response, including the route of administration, the bleomycin preparation, dose, mouse strain, age and so on. Prophylactic dosing schedules and non-conditional genetically-deficient mouse studies often report beneficial effects, but potentially not through a direct antifibrotic

response - instead by dampening the early inflammatory reaction to bleomycin. More therapeutically-targeted dosing regimens are infrequently employed (e.g. pirfenidone [6]; BIBF 1000 [7]; Imatinib [8]; prednisolone [9]), yet these have arguably provided a better prediction of clinical outcome.

Given the limited signal window of traditional fibrosis endpoints (such as high performance liquid chromatography (HPLC) determination of lung hydroxyproline), we employed μCT analysis of murine lungs *ex vivo* and established a quantitative *endpoint* measurement of fibrotic change following oropharyngeal bleomycin administration. Moreover, an appropriate window for applying a therapeutic dosing regimen to block fibrotic *progression* was determined, and successfully benchmarked using a small molecule inhibitor of TGFβR1/Activin receptor-like kinase 5 (ALK5) to block the signalling pathway downstream of the major pro-fibrotic cytokine, TGFβ. Using μCT, we also established that the fibrotic lesions did not completely resolve, but instead persisted for several months following a single insult with bleomycin.

MATERIALS AND METHODS

Detailed methods are provided in the online supplement.

Bleomycin animal model of lung injury

All animal studies were ethically reviewed and carried out in accordance with Animals (Scientific Procedures) Act 1986 and the GSK Policy on the Care, Welfare and Treatment of Animals. Bleomycin (50 IU/mouse in 50 µl sterile 0.9 % saline; Bleo-kyowa, Kyowa Hakko Ltd, UK) or saline was administered by oropharyngeal instillation to male C57Bl/6 mice (Charles River Laboratories, UK) as described previously [10]. The experimental groups are outlined in Table 1.

For real-time RT-PCR and total lung collagen measurements, lungs were snap-frozen in liquid nitrogen (and weighed). For µCT, histological and immunohistochemical analysis, lungs were insufflated and fixed; as described previously [10], although alternative fixation approaches exist for µCT imaging e.g. [11].

ALK5 inhibition studies with SB525334A

The highly selective small molecule ALK5 inhibitor, SB525334A [12], was a kind gift from GlaxoSmithKline, Stevenage, UK. Fourteen days post-bleomycin, SB525334A (30mg/kg in 100 µl acidified saline/0.2% Tween 80 pH 4.1) or vehicle (acidified

saline/0.2% Tween 80 pH 4.1) was administered twice daily by oral gavage, out to 28 days post-bleomycin (see Table 1 for experimental groups).

Determination of total lung collagen

Total lung collagen was determined by measuring hydroxyproline content in aliquots of pulverized lung as described previously [10]. Hydroxyproline was quantified by reverse-phase high performance liquid chromatography (HPLC) of 7-chloro-4-nitrobenzo-oxao-1,3,-diazole-derived acid hydrolysates. Total lung collagen was calculated assuming that collagen contains 12.2% (w/w) hydroxyproline and was expressed as mg per lung.

Total lung collagen was also measured using the Sircol™ assay (Biocolor Ltd, UK) according to the manufacturer's instructions, and expressed as mg per lung.

µCT scanning

Fixed, insufflated lungs were incubated for 2 hrs each in 70 %, 80 % and 90 % ethanol, then overnight in 100 % ethanol. Lungs were subsequently transferred to 100 % hexamethyldisilazane for a further 2 hrs, prior to air-drying. Lungs were then packaged for µCT scanning. Voxel sizes of 1-2 µm are feasible [11], but associated with prohibitively long scan/reconstruction times of several hours per sample. We opted for a voxel size of 13.7µm and a scan time of around 10 minutes, allowing high resolution visualisation and analysis of fibrosis, with good throughput. Lungs were scanned in a Skyscan 1072 µCT scanner (SkyScan, Belgium) at 40 kV/100 µA, without a filter, using two frame averaging and 0.9° angular rotation step size; based on the typical measured 10% Modulation Transfer Function (MTF) in the Skyscan

1072, spatial resolution was in the region of 20 - 30 µm. Reconstruction was carried out with the SkyScan NRecon software (Skyscan, Belgium).

µCT image analysis

Tissue segmentation analysis was performed using InForm™ software (Caliper Life Sciences, UK). Briefly, the software was "trained" to recognise fibrotic or normal lung, large airways, vessels and packaging material, using two representative µCT sections (8-bit greyscale) from each animal in the study. Segmentation was then carried out on a medium sample area at fine resolution, to measure the tissue volume and greyscale density of fibrotic and normal lung tissue for every µCT section. Data for each lung (~900 sections) were then compiled into a composite measurement of fibrosis (volume fibrosis x greyscale density) per whole lung.

Voxel Density Analysis

Composite 256-colour greyscale histograms (from 0 = black to 255 = white) were generated for each lung (excluding the large airways), representing the frequency distribution of pixel densities. The mean number of pixels in each bin (1 greyscale unit wide) were then calculated for each group, along with a t-test distribution showing the p-value for the comparison between each animal group at each greyscale bin. Greyscale density was not converted to Hounsfield Units due to the processing and dehydration required for our *ex vivo* analysis.

Histological analysis

For standard histological processing (H&E staining or Martius Scarlet Blue stain for collagen), 2 μm paraffin sections were cut and mounted on polylysine-coated glass slides and processed accordingly. All sections were subsequently scanned on a Nanozoomer and images were captured using NDP.view v1.2.36 (both from Hamamatsu Corporation, Japan). Direct comparisons between μCT and histology were performed on the same set of lungs; post-CT, lungs were rehydrated through an ethanol gradient (100%, 90%, 80% and 70%; 2 hours in each) prior to normal histological processing.

Real-time RT-PCR

Real-time qPCR was carried out as previously described [10], except that normalization used the geometric mean of the crossing point (Cp) values for two housekeeping genes: ATP Synthase 5B (ATP5B) and β2-microglobulin (B2M), identified by GeNorm analysis as the most stable housekeeping genes for this study. Statistics were calculated on the ΔCp values. All primers and GeNorm kits were purchased from Primer Design, Southampton, UK.

Statistical analysis

Statistical analysis was performed using SigmaPlot 12.3 software. Differences between two groups were evaluated by a two-tailed Student's t-test. Multiple group comparisons were evaluated using one- or two-way ANOVA as appropriate, with Holm-Sidak post hoc testing. Pearson's correlation was used to determine the

statistical significance of correlated data. A p-value of less than 0.05 was considered significant.

RESULTS

Delineation of the progressive fibrotic phase following bleomycin instillation

Our standard model of bleomycin-induced lung fibrosis (BILF) had typical endpoints for the inflammatory and fibrotic phases of 7 and 14 days, respectively (associated with a ~60 % increase in the amount of total lung collagen). We chose to assess changes in lung parameters over an extended timecourse, from 3 days to 28 days post bleomycin. In a separate experiment, we also assessed mice 3 months and 6 months after injury.

Total lung weight rose rapidly post bleomycin, peaking at 14 days (Figure 1A). At 3 months post bleomycin, lung weight was still significantly increased above control (mean ± SEM of bleo vs saline: 194 ± 3.4 mg vs 145 ± 3.9 mg, n = 8, $p<0.05$). HPLC determination of hydroxyproline content demonstrated that total lung collagen was significantly increased above baseline from day 10 onwards (Figure 1B), with a 65% increase in collagen at day 14, rising to a 91% increase in total lung collagen by day 28. In contrast, the commonly used Sircol™ assay gave a markedly different profile and magnitude of the changes in lung collagen (Supplementary Figure 1C), accounting for just 9% of the lung collagen determined by HPLC at day 28; no correlation was observed between HPLC and Sircol™ measures of lung collagen. Representative histological sections are depicted in Supplementary Figure 2.

The period from day 14 to day 28 therefore represents *progression* of established fibrosis, and was chosen as the optimal window of opportunity for therapeutic intervention in this model. Interestingly, total lung collagen remained significantly

elevated at 3 months post bleomycin, to the same extent (i.e. ~92% increase over baseline) as that seen at day 28, indicating a failure to reverse the increased deposition of lung collagen up to 12 weeks following a single bleomycin instillation.

Ex vivo µCT analysis of the temporal response to bleomycin

We sought to establish whether µCT could provide a more sensitive and reliable endpoint measure of fibrotic change for the entire lung *ex vivo*, compared with HPLC analysis of hydroxyproline or histologic analysis. Representative mid-lung transverse µCT sections and 3D volume renderings from day 14 to day 28 post bleomycin are shown in Figure 2. X-ray dense fibrotic lesions were clearly apparent, with a more apical and dorso-centric distribution attributable to the route of bleomycin distribution (Figure 2B and Supplementary Videos 1-4). Fibrosis was prominent around broncho-vascular bundles and extended out to the periphery; evidence of traction bronchiectasis, dense consolidation, interlobular septal thickening and subpleural scarring were also easily discernible.

Activin receptor-like Kinase 5 (ALK5) inhibition during the progressive phase of fibrosis

As a proof of concept for quantifying the degree of fibrosis evident on µCT after an appropriately timed therapeutic intervention, a highly potent and selective small molecule inhibitor of TGFβRI (ALK5), SB525334A, was given twice daily by oral gavage from day 14, once fibrosis was already well-established, until day 28.

Bleomycin injury resulted in increased lung weight at day 28, but no significant differences were seen between the vehicle and ALK5 inhibitor groups (Figure 3A). However, therapeutic ALK5 inhibition significantly attenuated the BILF at day 28, as evidenced by HPLC determination of lung hydroxyproline (Figure 3B). SB525334A significantly reduced (by ~55%), but did not fully reverse, the increased deposition of lung collagen.

μCT detected extensive fibrotic change, which fully matched the equivalent histological sections (Figure 3E and F). We utilised a pattern recognition approach with InForm™ software (Caliper Life Sciences, UK) to segment the tissue into normal parenchyma and fibrotic lesions (excluding extraneous fascia or packaging material), for all ~14,000 μCT sections from the study (Figure 3D). We calculated the volume of lung occupied by fibrotic lesion, and its associated greyscale CT density, to create a composite measure of 'volume x density' encompassing both the extent and severity of fibrosis (Figure 3C). μCT gave a much greater window for detecting fibrotic change compared with lung hydroxyproline, but the therapeutic effects of ALK5 inhibition were equivalent (~60% reduction in fibrosis compared with bleomycin alone).

We also performed a simple voxel density analysis of each lung, without relying on segmentation into normal and fibrotic regions. Histograms were generated showing the mean number of voxels per lung, at each greyscale value from 0 (least dense) to 255 (most dense, Figure 4A and B). The 'Bleo + Vehicle' group had an increased proportion of higher greyscale values (indicative of higher density on CT) compared with the 'Saline + Vehicle' group. In comparison with the 'Bleo + Vehicle' group, the 'Bleo + SB525334A' mice clearly had significantly fewer voxels in the density range 42 - 137, indicating a lesser degree of fibrosis (Figure 4B and C). No significant

differences were detected between ‘Saline + Vehicle’ and the ‘Saline + SB525334A’ groups (not shown).

µCT quantification of lungs three and six months post-bleomycin

We also used µCT to address the question of resolution and restoration of normal lung architecture following a single instillation of bleomycin. At both 3 and 6 months post bleomycin, the persistence of fibrotic change (reminiscent of fibrotic organising pneumonia) was still obvious by µCT, with thickening of interlobular septae and a lace-like pattern of fibrosis, enlarged airspaces, thickened subpleura and a massively distorted lung outline – indicating failure to fully resolve the BILF or completely restore the normal lung architecture (Figure 5B&C, Figure 6 and Supplementary Videos 5&6). µCT therefore revealed gross lung abnormalities which persisted for an extensive period following a single instillation of bleomycin. Histological examination demonstrated the presence of hyperplastic epithelium and/or bronchiolization, and highly disturbed alveolar architecture. The ‘volume x density’ readout by µCT was significantly higher than control at both 3 and 6 months post bleomycin (Figure 5A). There was however a significant diminution in this parameter at 6 months compared with 3 months, suggesting partial re-modeling of the fibrotic change.

DISCUSSION

To the best of our knowledge, this is the most thorough characterization and benchmarking of the bleomycin model of lung fibrosis performed to date, using a cutting-edge μCT scanning and analytical approach to define a novel and sensitive endpoint for pre-clinical drug evaluation. Identification of new therapies for the treatment of a disease such as IPF is very much dependent on the ability of experimental models to predict the eventual clinical outcome.. In many studies (including our own previous work), prophylactic dosing schedules and/or the use of non-conditional genetically-deficient mice have suggested the anti-fibrotic potential of a vast array of drug targets and key fibrotic pathways [3], yet the overwhelming majority of clinical trials have failed to reproduce the hoped for translation of therapeutic benefit from mouse to man.

The more limited number of studies where therapeutic dosing strategies have been employed, arguably provide more clinically relevant data. Pirfenidone, for example, shows efficacy when dosed therapeutically during bleomycin-induced lung fibrosis in hamsters and mice [6;13], and has received marketing authorization for the treatment of mild-to-moderate IPF in Europe. In contrast, oral prednisolone given therapeutically to rats following bleomycin administration, does not ameliorate fibrosis [9;14]. A recent clinical trial of the tyrosine kinase inhibitor, Imatinib, failed to demonstrate any beneficial effects on survival or lung function in IPF [15]; therapeutic dosing of Imatinib in mice following bleomycin exposure also failed to show efficacy [8]. One could argue therefore that the experimental model of lung fibrosis induced by bleomycin may have the potential to be predictive of clinical outcome, if appropriate dosing strategies and endpoints are employed.

In this study we have carefully defined a window of opportunity between 14 and 28 days after a single oropharyngeal instillation of bleomycin (50 IU per mouse in 50µl saline), where there is *progression* of the established fibrotic lesions, as defined by a further increase in the amount of total lung collagen and a maturation of the deposited collagen fibres on histology. Although this represents a rapid and acute worsening of the fibrosis, the underlying pathomechanisms are likely relevant in terms of human disease.

Small animal imaging, using µCT, volumetric flat panel CT[16], or magnetic resonance imaging (MRI)[17], for example, is gaining in popularity for investigating morphological changes in the murine lung. Since these are minimally invasive and non-destructive approaches, they can also be applied to longitudinally investigate the development of lung fibrosis in mice and rats *in vivo* - however, the degree of resolution is constrained by respiratory and cardiac motion [18] and, for CT, the dose of radiation which can safely be administered. Our *ex vivo* µCT scanning approach clearly identified the fibrotic lesions from 14 days onwards, with a highly reproducible mid- to upper-lung and dorso-centric distribution pattern, and negated the practical and analytical difficulties associated with imaging live animals - thereby opening up the adoption of this methodology by other laboratories. Moreover, by analysing the whole lung we avoided the sampling error/bias associated with histologic analyses [19].

Elegant studies have compared/contrasted *in vivo* and *ex vivo* µCT scanning of normal murine lungs [11], or highlighted differences in lung structure between mouse strains [20]. Few studies, however, have addressed the use of µCT for evaluation of

the degree of fibrotic change in murine models of lung fibrosis. Previous studies [21-23] used *in vivo* μCT to investigate fibrotic changes in the AdTGFβ1-induced or bleomycin models of lung fibrosis in rats or mice with associated voxel sizes of approximately 155 μm, 94 μm or 35 μm respectively. These studies used different approaches to segment the tissue into either fibrotic [21] or aerated lung volumes [22], or used semi-quantitative pathological scoring [23], but the utility of these approaches has not yet been validated with a drug intervention strategy. A recent study by Jin *et al* used μCT (with ~44.25 μm spatial resolution) to investigate the therapeutic effects of rosiglitazone during BILF in mice [24]; they reported beneficial changes in a qualitative radiological assessment, but did not provide a fully quantitative measure of fibrotic change. It is worth mentioning that the study by Ask *et al* [21] also investigated lung function (pressure-volume loops on mechanical ventilation) and demonstrated a strong correlation between lung stiffness and the degree of fibrosis on μCT – highlighting that lung function parameters are also a highly relevant endpoint measure in fibrosis models.

Our μCT study has been benchmarked using a carefully conducted therapeutic dosing strategy with a TGFβR1 kinase (ALK5) inhibitor. ALK5 inhibition was selected as an appropriate proof-of-concept, given the undisputed importance of the TGFβ signalling pathway as a major driver of the pro-fibrotic response; ALK5 inhibition with the small molecule inhibitor SD-208 was shown to be of therapeutic benefit in the AdTGFβ1-induced model of lung fibrosis [25], while prophylactic dosing with SB525334A attenuated various histopathological alterations of the fibrotic lung during BILF [26]. In line with the SD-208 data, our therapeutic dosing strategy with SB525334A also significantly attenuated fibrotic progression. Dosing commenced when the lungs would already have had a ~60% increase in total lung collagen (i.e.

at 14 days post bleomycin); ALK5 inhibition completely blocked the expected progression, validating the major pro-fibrotic role of TGFβ signalling. HPLC determination of total lung collagen and μCT evaluation of fibrosis were in close agreement in terms of the efficacy of SB525334A - with a roughly 55 - 60% attenuation of the fibrotic response. Importantly however, μCT gave a larger window for detecting a therapeutic effect. Significantly, this response was determined with as few as 3 – 4 mice per group, in contrast to the 8 – 11 mice normally used for HPLC determination, thus reducing the number of experimental animals required; moreover, the same lungs used for μCT could then be processed for histological examination – further refining and reducing the required number of mice. The approach is necessarily dependent on a highly standardized and homogeneous lung insufflation/fixation protocol to avoid misclassification of tissue artefacts; however, in a separate study, HPLC analysis of lung hydroxyproline was also successfully performed on lungs immediately after μCT analysis (rather than histology), and revealed a significant correlation between total lung collagen and μCT evaluation (r^2 = 0.7553, $p<0.001$). In terms of radiological assessment, μCT clearly highlighted areas of dense consolidation, traction bronchiectasis, interlobular septal thickening and subpleural scarring – and these areas corresponded perfectly to areas of fibrosis identified histologically. This work lends further support to the validity and improved sensitivity of μCT as a true outcome measure of fibrotic severity in BILF.

Of interest, we also assessed the commonly used Sircol™ assay during the temporal response to bleomycin. The proportion of lung collagen detected by Sircol™ accounted for only 9% of the total lung collagen determined by HPLC analysis. No correlation between the two measures was determinable. Moreover, Sircol™ revealed an increase in the collagen signal at 7 days post bleomycin, which was not

reproduced by HPLC determination. In a recent paper by Lareu *et al* [27], a detailed analysis of the Sircol™ assay highlighted a problem due to interference of non-collagenous proteins such as serum proteins, unless the protocol is appropriately modified; we would speculate that the increased Sircol™ signal at day 7 may therefore reflect increased vascular leak at this timepoint [10], and would question the validity of the Sircol™ assay as a standalone endpoint measure of fibrosis, unless appropriately modified.

A major criticism of BILF as a model of IPF is the widespread acceptance that the fibrotic lesions resolve rapidly, often within 5 to 6 weeks following bleomycin administration [28;29] - which is clearly at odds with the human condition which is chronic and progressive. Our data instead showed that while the fibrotic lesions do not continue to progress, they do persist for at least six months following a single oropharyngeal instillation of bleomycin. Indeed, at three months post-bleomycin, the increase in total lung collagen was equivalent to that seen at 28 days, implying little or no resolution of the fibrotic response in this timeframe. By six months post-bleomycin, μCT continued to reveal the presence of an highly altered lung architecture, reminiscent of fibrotic organising pneumonia, and associated with fibrosis around bronchovascular bundles, subpleural scarring and a massively distorted lung outline. Histologically, the overall cellularity of the fibrotic lesions appeared decreased (in terms of inflammatory infiltrate and fibroblasts), and they were instead composed of dense bands of scar tissue, associated with abundant hyperplastic epithelium and/or bronchiolization – which are histological hallmarks of IPF. Previously, hyperplastic epithelium has only been consistently observed in a repetitive bleomycin dosing model [30]. Our data suggest that these features are associated with remodelling of the fibrosis, but there does not appear to be a marked

restoration of the alveolar architecture at this late timepoint. Under these conditions therefore, we do not observe complete resolution of the fibrotic response to bleomycin, which opens up the possibility for assessing therapeutic approaches capable of initiating lung repair, rather than just halting fibrosis. Our data also reiterate the temporal heterogeneity of the fibrotic response instigated by the various permutations of the bleomycin model [5].

In conclusion, this work demonstrates that the experimental model of lung fibrosis induced by oropharyngeal bleomycin administration can be a highly useful model for establishing the therapeutic efficacy of target compounds to block fibrotic progression of lesions which do not rapidly resolve. It also highlights the importance of a thorough characterization of each laboratory's permutation of the bleomycin model, to define the most appropriate dosing strategies and to understand the natural history of the fibrotic response and associated fibrogenic mechanisms.

ACKNOWLEDGEMENTS

We would especially like to thank Dr Penny Shaw, Consultant Radiologist at University College London Hospital, for expert evaluation and interpretation of the μCT data. We would also like to thank Mr Steve E. Bottoms for expert technical assistance with histology. The authors are grateful to the following grant agencies for funding: British Lung Foundation (C.J.S. Research Fellowship F07/6); Medical Research Council (C.J.S. Career Development Award G0800340; R.C.C. CASE Award 2009–12); Wellcome Trust (A.D. Clinical Research Training Fellowship 084382/Z/07/Z); European Commission (R.C.C Framework 7 Programme HEALTH-F2- 2007-2224; European IPF Network).

AUTHOR CONTRIBUTIONS

CJS, BH, REA, AD and EJF acquired the data; CJS, PM and RCC conceived & designed the studies; CJS, PM, EJF and BH analyzed & interpreted the μCT data; CJS, RAE, AD and EJF generated and analysed the hydroxyproline data; CJS and RCC drafted or revised the manuscript. All authors reviewed and commented upon the manuscript.

ONLINE SUPPORTING INFORMATION

Detailed methods, additional results, two supplementary figures and eight supplementary videos are also provided as online-only files.

REFERENCES

1. Coultas DB, Zumwalt RE, Black WC, Sobonya RE. The epidemiology of interstitial lung diseases. *Am J Respir Crit Care Med* 1994; 150(4):967-72.

2. Datta A, Scotton CJ, Chambers RC. Novel therapeutic approaches for pulmonary fibrosis. *Br J Pharmacol* 2011; 163(1):141-72.

3. Moeller A, Ask K, Warburton D, Gauldie J, Kolb M. The bleomycin animal model: a useful tool to investigate treatment options for idiopathic pulmonary fibrosis? *Int J Biochem Cell Biol* 2008; 40(3):362-82.

4. Moore BB, Hogaboam CM. Murine models of pulmonary fibrosis. *Am J Physiol Lung Cell Mol Physiol* 2008; 294(2):L152-L160.

5. Scotton CJ, Chambers RC. Bleomycin revisited: towards a more representative model of IPF? *Am J Physiol Lung Cell Mol Physiol* 2010; 299(4):L439-L441.

6. Kakugawa T, Mukae H, Hayashi T, Ishii H, Abe K, Fujii T, et al. Pirfenidone attenuates expression of HSP47 in murine bleomycin-induced pulmonary fibrosis. *Eur Respir J* 2004; 24(1):57-65.

7. Chaudhary NI, Roth GJ, Hilberg F, Muller-Quernheim J, Prasse A, Zissel G, et al. Inhibition of PDGF, VEGF and FGF signalling attenuates fibrosis. *Eur Respir J* 2007; 29(5):976-85.

8. Aono Y, Nishioka Y, Inayama M, Ugai M, Kishi J, Uehara H, et al. Imatinib as a novel antifibrotic agent in bleomycin-induced pulmonary fibrosis in mice. *Am J Respir Crit Care Med* 2005; 171(11):1279-85.

9. Chaudhary NI, Schnapp A, Park JE. Pharmacologic differentiation of inflammation and fibrosis in the rat bleomycin model. *Am J Respir Crit Care Med* 2006; 173(7):769-76.

10. Scotton CJ, Krupiczojc MA, Konigshoff M, Mercer PF, Lee YC, Kaminski N, et al. Increased local expression of coagulation factor X contributes to the fibrotic response in human and murine lung injury. *J Clin Invest* 2009; 119(9):2550-63.

11. Vasilescu DM, Knudsen L, Ochs M, Weibel ER, Hoffman EA. Optimized murine lung preparation for detailed structural evaluation via micro-computed tomography. *J Appl Physiol* 2012; 112(1):159-66.

12. Grygielko ET, Martin WM, Tweed C, Thornton P, Harling J, Brooks DP, et al. Inhibition of gene markers of fibrosis with a novel inhibitor of transforming growth factor-beta type I receptor kinase in puromycin-induced nephritis. *J Pharmacol Exp Ther* 2005; 313(3):943-51.

13. Iyer SN, Margolin SB, Hyde DM, Giri SN. Lung fibrosis is ameliorated by pirfenidone fed in diet after the second dose in a three-dose bleomycin-hamster model. *Exp Lung Res* 1998; 24(1):119-32.

14. McGrath EE, Millar AB. Hot off the breath: triple therapy for idiopathic pulmonary fibrosis--hear the PANTHER roar. *Thorax* 2012; 67(2):97-8.

15. Daniels CE, Lasky JA, Limper AH, Mieras K, Gabor E, Schroeder DR. Imatinib treatment for idiopathic pulmonary fibrosis: Randomized placebo-controlled trial results. *Am J Respir Crit Care Med* 2010; 181(6):604-10.

16. Wielputz MO, Eichinger M, Zhou Z, Leotta K, Hirtz S, Bartling SH, et al. In vivo monitoring of cystic fibrosis-like lung disease in mice by volumetric computed tomography. *Eur Respir J* 2011; 38(5):1060-70.

17. Babin AL, Cannet C, Gerard C, Wyss D, Page CP, Beckmann N. Noninvasive assessment of bleomycin-induced lung injury and the effects of short-term glucocorticosteroid treatment in rats using MRI. *J Magn Reson Imaging* 2011; 33(3):603-14.

18. Bartling SH, Kuntz J, Semmler W. Gating in small-animal cardio-thoracic CT. *Methods* 2010; 50(1):42-9.

19. Hsia CC, Hyde DM, Ochs M, Weibel ER. An official research policy statement of the American Thoracic Society/European Respiratory Society: standards for quantitative assessment of lung structure. *Am J Respir Crit Care Med* 2010; 181(4):394-418.

20. Thiesse J, Namati E, Sieren JC, Smith AR, Reinhardt JM, Hoffman EA, et al. Lung structure phenotype variation in inbred mouse strains revealed through in vivo micro-CT imaging. *J Appl Physiol* 2010; 109(6):1960-8.

21. Ask K, Labiris R, Farkas L, Moeller A, Froese A, Farncombe T, et al. Comparison between conventional and "clinical" assessment of experimental lung fibrosis. *J Transl Med* 2008; 6:16.

22. Rodt T, von FC, Dettmer S, Halter R, Maus R, Ask K, et al. Micro-computed tomography of pulmonary fibrosis in mice induced by adenoviral gene transfer of biologically active transforming growth factor-beta1. *Respir Res* 2010; 11:181.

23. Lee HJ, Goo JM, Kim NR, Kim MA, Chung DH, Son KR, et al. Semiquantitative measurement of murine bleomycin-induced lung fibrosis in in vivo and postmortem conditions using microcomputed tomography: correlation with pathologic scores--initial results. *Invest Radiol* 2008; 43(6):453-60.

24. Jin GY, Bok SM, Han YM, Chung MJ, Yoon KH, Kim SR, et al. Effectiveness of rosiglitazone on bleomycin-induced lung fibrosis: Assessed by micro-computed tomography and pathologic scores. *Eur J Radiol* 2012; 81(8):1901-6.

25. Bonniaud P, Margetts PJ, Kolb M, Schroeder JA, Kapoun AM, Damm D, et al. Progressive transforming growth factor beta1-induced lung fibrosis is blocked by an orally active ALK5 kinase inhibitor. *Am J Respir Crit Care Med* 2005; 171(8):889-98.

26. Higashiyama H, Yoshimoto D, Kaise T, Matsubara S, Fujiwara M, Kikkawa H, et al. Inhibition of activin receptor-like kinase 5 attenuates bleomycin-induced pulmonary fibrosis. *Exp Mol Pathol* 2007; 83(1):39-46.

27. Lareu RR, Zeugolis DI, Abu-Rub M, Pandit A, Raghunath M. Essential modification of the Sircol Collagen Assay for the accurate quantification of collagen content in complex protein solutions. *Acta Biomater* 2010; 6(8):3146-51.

28. Chung MP, Monick MM, Hamzeh NY, Butler NS, Powers LS, Hunninghake GW. Role of repeated lung injury and genetic background in bleomycin-induced fibrosis. *Am J Respir Cell Mol Biol* 2003; 29(3 Pt 1):375-80.

29. Lawson WE, Polosukhin VV, Stathopoulos GT, Zoia O, Han W, Lane KB, et al. Increased and prolonged pulmonary fibrosis in surfactant protein C-deficient mice following intratracheal bleomycin. *Am J Pathol* 2005; 167(5):1267-77.

30. Degryse AL, Tanjore H, Xu XC, Polosukhin VV, Jones BR, McMahon FB, et al. Repetitive intratracheal bleomycin models several features of idiopathic pulmonary fibrosis. *Am J Physiol Lung Cell Mol Physiol* 2010; 299(4):L442-L452.

FIGURE LEGENDS

Figure 1. Timecourse of increase in lung weight and total lung collagen following bleomycin instillation. (**A**) Lung weight increased rapidly after bleomycin injury, with a significant increase at day 3 post injury, attributable to vascular leak and lung oedema, which was further augmented by day 7 and then maintained at a relatively stable level until day 28 - despite a concomitant decline in the degree of vascular leak in this model [10]. (**B**) Total lung collagen (HPLC determination of hydroxyproline) was significantly increased from day 10 to day 28; in a separate cohort of mice, the lung collagen content at 3 months post-bleomycin showed no diminution from the corresponding value at 28 days. There was a significant correlation between lung weight and total lung collagen at day 28 ($r^2 = 0.69$; $p<0.01$). All data are mean ± SEM. * $p<0.05$; ** $p<0.01$; *** $p<0.001$ (ANOVA) versus matched timepoint control. n = 8 - 11 mice per group.

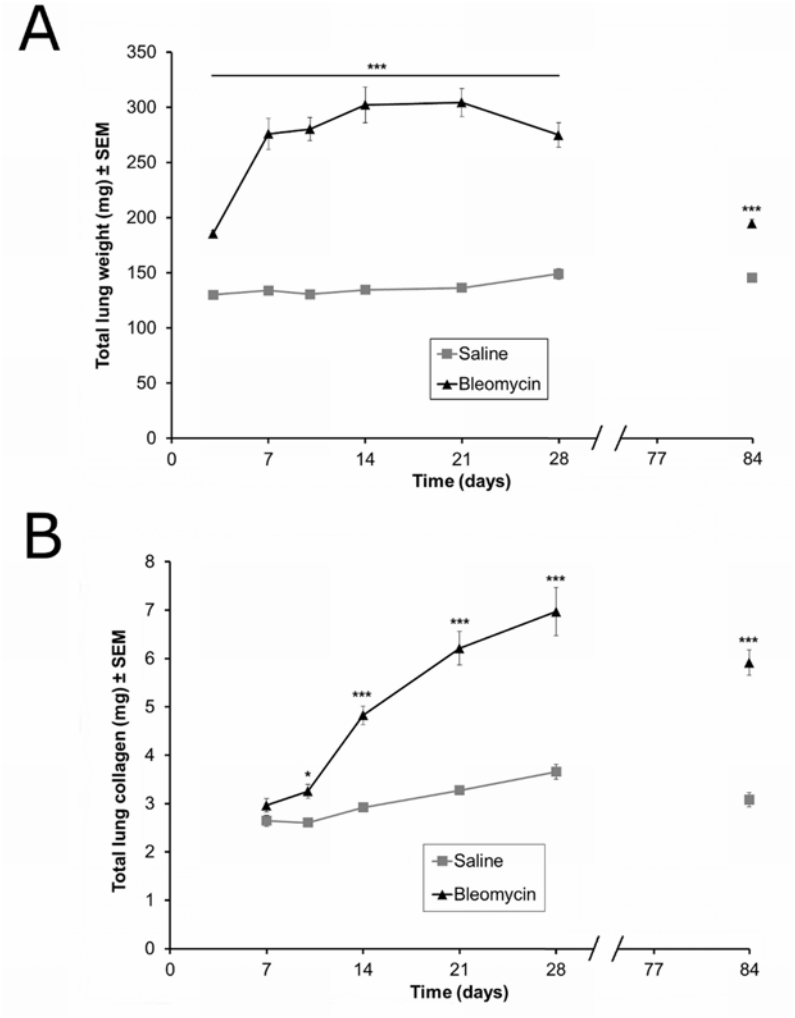

Figure 2. *Ex vivo* µCT lung images following bleomycin instillation. (A) Representative mid-lung transaxial µCT sections from day 14 to day 28 post saline/bleomycin instillation. Fibrotic regions comprising dense consolidation, traction bronchiectasis and subpleural scarring are highly evident in every lobe of lungs injured by bleomycin instillation. By day 28, the lung outline becomes distorted, which is particularly apparent on the dorsal (lower) surface. For orientation, the oesophagus (oe) and main bronchi (br) are labelled on the day 14 saline section. Day 21 post-bleomycin has an inset showing an enlargement (3x) of the area bounded by the box, to highlight a region with traction bronchiectasis and dense

consolidation, extending to the periphery of the lobe and adjacent to another lobe showing relatively normal lung tissue. (B) 3D volume reconstructions of bleomycin-injured lungs from day 14 to day 28, highlighting the reproducible dorso-centric lesion distribution. All scale bars are 1 mm.

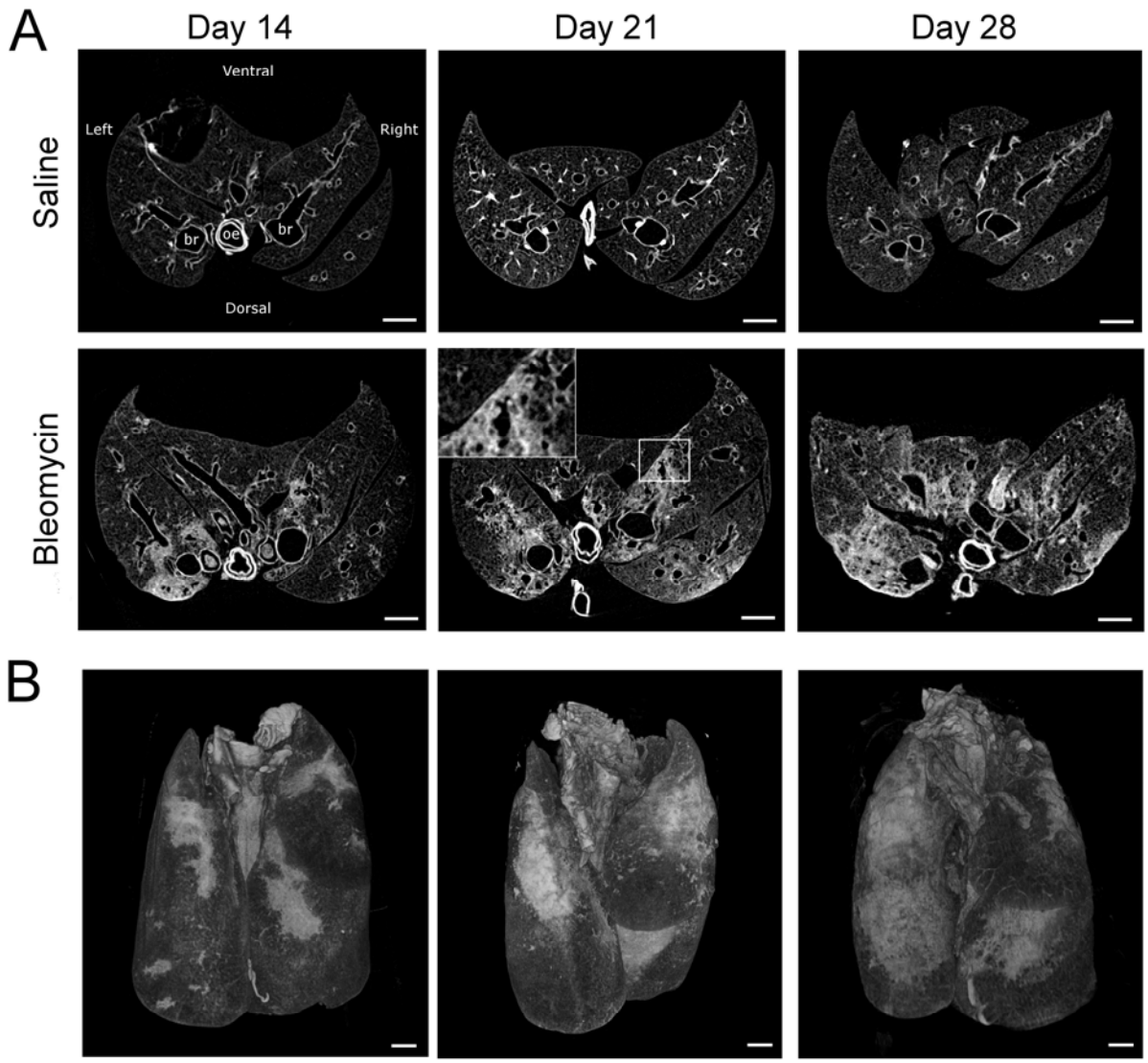

Figure 3. Therapeutic intervention during established fibrosis. (**A**) Total lung weight at day 28 following bleomycin was significantly higher than in saline treated mice, but treatment with SB525334A by oral gavage *bid* from day 14 onwards did not

attenuate the increase in lung weight. (**B**) Total lung collagen accumulation (HPLC determination of hydroxyproline) at day 28 was, however, significantly abrogated by treatment with SB525334A. (**C**) InForm™ software analysis of the µCT sections showed a significant increase in the fibrosis 'volume x density' after bleomycin injury, which was also abrogated by SB525334A. (**D**) Representative transaxial µCT section (upper image) and the corresponding segmented image (lower image) from the InForm™ software, showing pattern recognition of fibrosis (red), normal lung (green) and major airways/vessels (blue). An asterix identifies CT signal from packaging material. (**E**) Fibrotic change on µCT (upper image; coronal section) correlated perfectly with the collagen deposition (blue colour) seen in the corresponding Martius Scarlet Blue-stained histological section (lower image); Scale bar: 5 mm. (**F**) Higher power view of a fibrotic area from (**E**); Scale bar: 0.5 mm. All data are mean ± SEM. * $p<0.05$; ** $p<0.01$; *** $p<0.001$ (ANOVA). n = 6 - 8 mice for hydroxyproline, n = 3 - 4 mice for µCT.

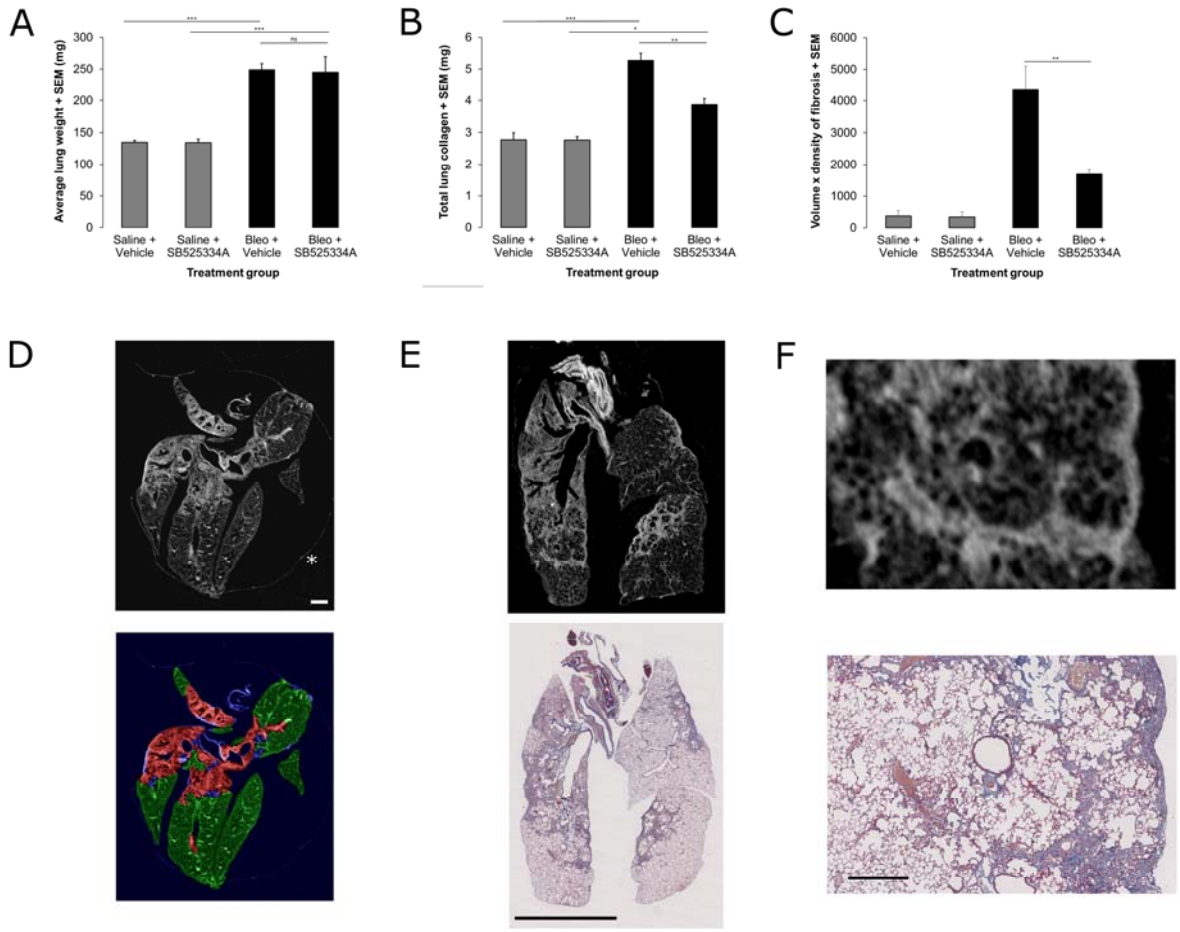

Figure 4. Voxel density analysis of µCT data. (A) Histograms were plotted of voxel numbers at each greyscale density value (1 to 255); for clarity, data for a greyscale value of 0 (i.e. air) are excluded. The bleomycin and saline groups deviate at higher greyscale values, with a greater number of dense voxels due to bleomycin injury (indicative of dense fibrosis). (B) The difference in number of voxels between the Bleo+Vehicle and Saline+Vehicle groups (red line) is clearly apparent; the Bleo+SB525334A group has fewer voxels in this density range in comparison with the Bleo+Vehicle group (blue line; corrected for controls), which reaches statistical significance (C) at greyscale values from 42 - 137. (D & E) This greyscale range (red

pixels) represents airway walls in a Saline+Vehicle µCT slide (D), and dense fibrosis and airway walls in a Bleo+Vehicle µCT slice (E). Scale bars: 1 mm.

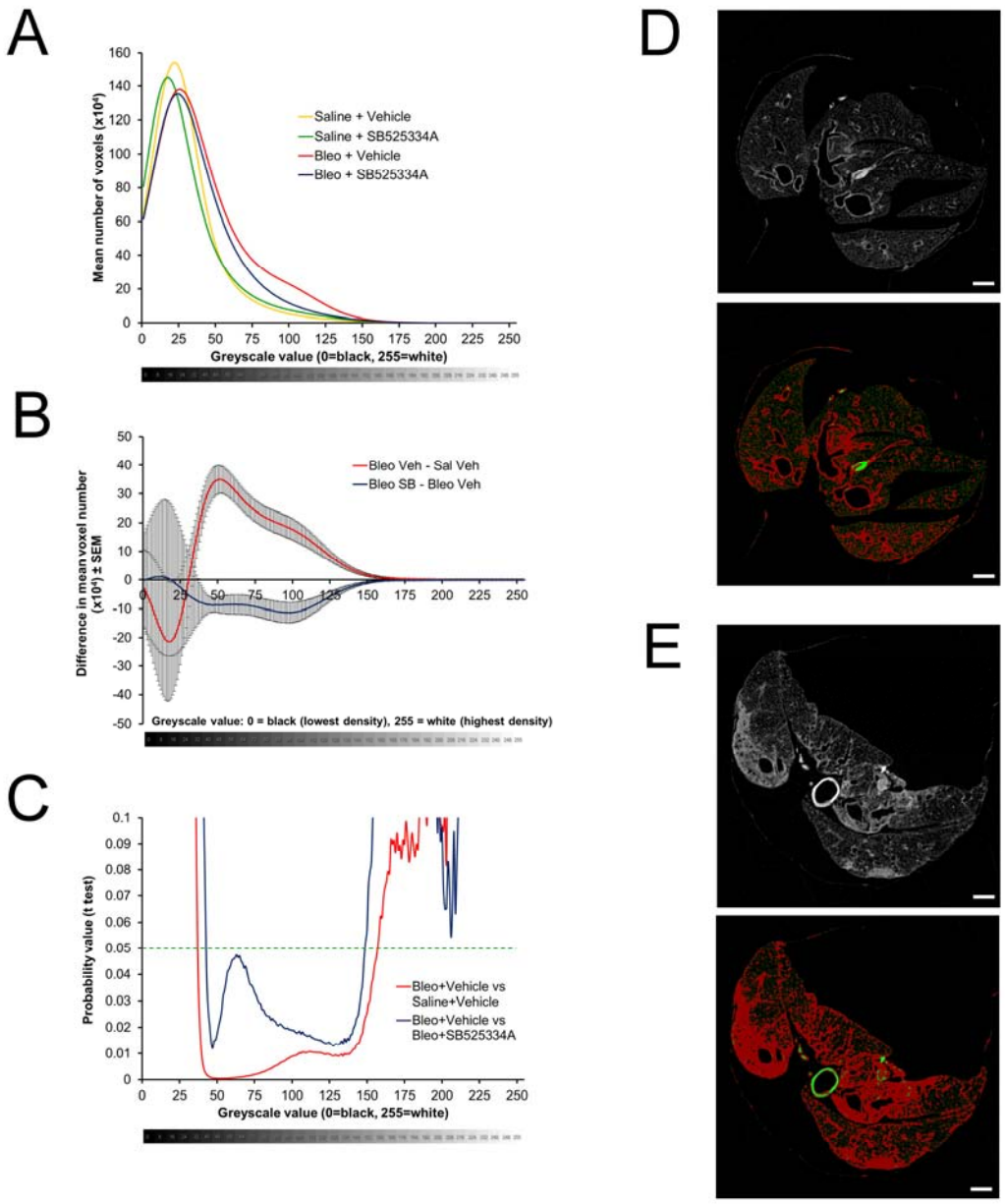

Figure 5. InForm™ image analysis of µCT data at longer timepoints following bleomycin injury. (**A**) The same InForm™ image analysis was applied to µCT scans 3 and 6 months post bleomycin. Significantly increased 'volume x density' of

fibrosis were observed, equivalent to data at days 21 and 28 (Fig. 3B and data not shown), showing that fibrotic lesions persist for at least 6 months following a single instillation of bleomycin in this model. (**B** & **C**) Representative 3D volume reconstructions and dorsal coronal CT sections from lungs 3 months and 6 months post-bleomycin, respectively, showing evidence for persistent fibrotic lesions, with a lace-like appearance reminiscent of fibrotic organising pneumonia. Scale bar: 1 mm. n = 4 mice per group.

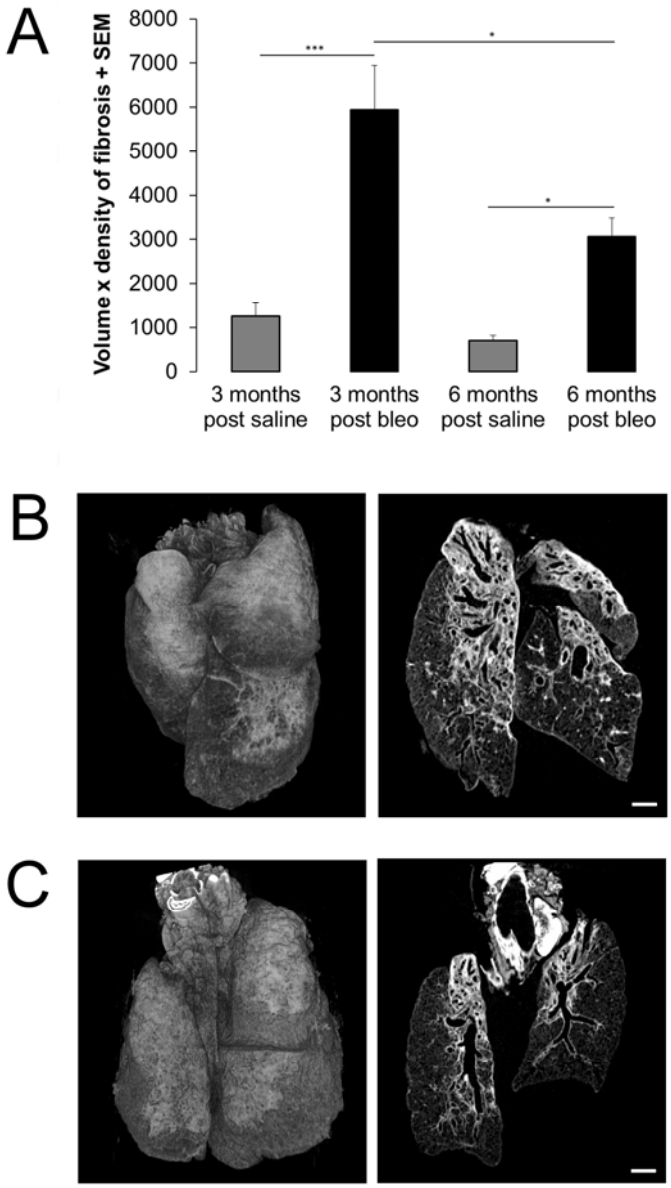
A
Volume x density of fibrosis + SEM
8000
7000
6000
5000
4000
3000
2000
1000
0
***
*
*
3 months post saline
3 months post bleo
6 months post saline
6 months post bleo
B
C

Figure 6. Histological appearance of lungs three and six months post-saline/bleomycin. (**A & B**) MSB stained section of a control lung 3 months post-saline reveals normal lung architecture at low (A) and high (B) power, respectively. (**C-F**) 3 months post-bleomycin, gross abnormality of the lung architecture is still apparent, with a highly distorted lung outline apparent at low power (C). At higher power (D and F), there is clear evidence of hyperplastic epithelium/bronchiolisation, dense bands of mature scar tissue surrounding the bronchovascular bundles (F) and frequent lymphocytic infiltrates (F). The equivalent mid-upper lung transaxial μCT section is also shown (E). (**G-H**) MSB stained section of a control lung 6 months post-saline reveals normal lung architecture at low (G) and high (H) power, respectively. (**I-K**) By 6 months post-bleomycin, fibrotic lesions were still evident and the lung outline remained severely distorted as shown at low power (I). Hyperplastic epithelium was particularly evident in areas of milder fibrosis, as shown here (J), suggesting an association with repair of the dense lesions. Overall cellularity appears diminished, but dense bands of scar tissue remain (L). The equivalent mid-upper lung transaxial μCT section is also shown in (K). All sections stained with Martius Scarlet Blue. For low power sections, scale bar = 2 mm; high power sections, scale bar = 100 μm (boxes on low power sections show location of magnified areas).

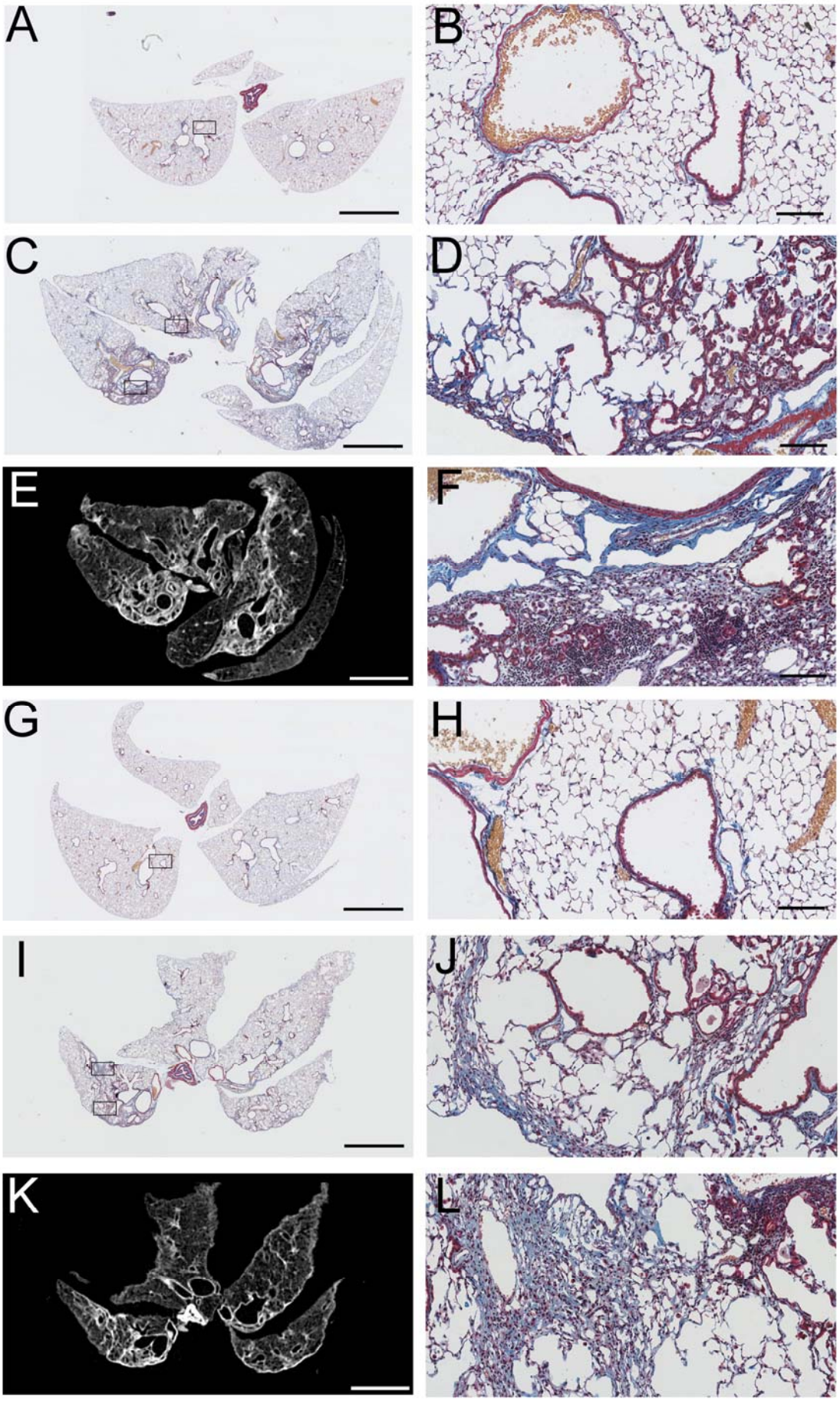
A
B
C
D
E
F
G
H
I
J
K
L

Experiment	Timepoint (days post saline/bleomycin)	Treatment	Total number of mice per group	Endpoint analysis
Timecourse of fibrotic response to bleomycin (bleo)	3	Saline control (Saline)	13	Biochemistry (10); Histology (3)
	3	Bleomycin injury (bleo)	14	Biochemistry (11); Histology (3)
	7	Saline	13	Biochemistry (10); Histology (3)
	7	Bleo	14	Biochemistry (11); Histology (3)
	10	Saline	11	Biochemistry (8); Histology (3)
	10	Bleo	12	Biochemistry (9); Histology (3)
	14	Saline	14	Biochemistry (10); Histology/μCT (4)
	14	Bleo	13	Biochemistry (8); Histology/μCT (5)
	21	Saline	14	Biochemistry (10); Histology/μCT (4)
	21	Bleo	13	Biochemistry (8); Histology/μCT (5)
	28	Saline	15	Biochemistry (10); Histology/μCT (5)
	28	Bleo	14	Biochemistry (9); Histology/μCT (5)
Determination of resolution post bleomycin injury	84	Saline	15	Biochemistry (8); Histology/μCT (7)
	84	Bleo	15	Biochemistry (8); Histology/μCT (7)
	168	Saline	4	Histology/μCT (4)
	168	Bleo	4	Histology/μCT (4)
Investigation of therapeutic effects of ALK5 inhibitor (dosed from day 14 to day 28 post bleomycin)	28	Saline + Vehicle	8	Biochemistry (5); Histology/μCT (3)
	28	Saline + SB525334A	8	Biochemistry (5); Histology/μCT (3)
	28	Bleo + Vehicle	12	Biochemistry (8); Histology/μCT (4)
	28	Bleo + SB525334A	11	Biochemistry (7); Histology/μCT (4)

Table 1. Details of *in vivo* experimental groups, timepoints, mouse numbers and endpoint analyses.